Eu_2O_3 microsphere luminescent material based on aerosol jet printing

Xiuyan Xu[1a*]

[1]Department of Energy and Environment, Southeast University, Nanjing, Jiangsu 210096, China

Abstract—In this paper, microsphere structural materials of europium oxide (Eu2O3) were prepared using the aerosol jet printing technique. Europium oxide powders were produced at different calcination temperatures for the comparisons of nanostructures and luminescence properties. The peak of the emission spectrum of Eu^{3+} is near 612 nm (red), which contributes to the three primary colors. As an important and typical rare earth oxide, Eu_2O_3 plays an important role in red phosphor materials and is an activator for the red phosphor. Rare earth oxides microsphere materials are widely used in modern industrial production, such as light, electricity, magnetism, mechanics, and machinery, because of their advantages of the small size effect and the surface effect. Eu_2O_3 microsphere nanomaterials possess the advantages of both rare earth oxides and microsphere materials, exhibiting excellent optical properties and laying a good foundation for the development of biomedical, electronic information photocatalysis and other industries. However, the existing preparation methods of Eu_2O_3 microsphere nanomaterials have shortcomings, including uncontrollable microparticle morphology and complicated experimental operations. The most important point is that the initial pattern of the phosphor cannot be customized, and a secondary process is needed to obtain the target pattern. This two-step process inevitably leads to the loss of material and production time. Under this background, this experiment attempts to prepare a microspherical Eu_2O_3 phosphor using aerosol jet printing (AJP) technology, which is an important attempt to improve the level of the luminescent performance and the customization level of the fluorescent initial pattern.

1. Introduction

In recent years, rare earth oxide microsphere structure materials have received growing attention due to their key features, such as higher bulk density, larger surface area and unique 4f electrons, exhibiting outstanding performance in biopharmaceuticals, electronic information, medical devices, light-emitting materials and other modern industries [1]. The 4f electron orbitals of rare earth elements are unfilled [2], and the internal electrons are easy to transmit. The most widely studied rare earth oxide is Eu_2O_3 as a result of its strong fluorescence emission, high purity of emitted light and long lifetime [3], which is widely used in the field of daily life ranging from flat panel displays and LED lighting to the chemical industry. The $^5D_0 \rightarrow ^7F_J$ (J=0,1,2,3 and 4) electronic transitions lead to the emission band of Eu_2O_3 centered at approximately 612 nm, which is an important activator of red fluorescent materials [4]. Eu^{3+} ions are sensitive to the symmetry of the lattice environment. In the range of 550-720 nm, the source of the $^5D_0 \rightarrow ^7F_1$ (590 nm) magnetic transition is Eu^{3+} ions occupying the centrosymmetric lattice sites [5]. The Eu^{3+} ion disorder in the lattice promotes the degree of the $^5D_0 \rightarrow ^7F_2$ (612 nm) electronic transition at $^5D_0 \rightarrow ^7F_J$ [5]. The traditional processes for the preparation of nanopor materials are sol-gel, aqueous/solvent thermal, radio frequency sputtering, pulsed laser deposition and template methods (hard template, soft template, sacrificial template, etc.) and template-free methods (spray reaction, emulsion drop, etc.) [6]. However, the two contradictions of irregular particle morphology and energy consumption, regular spherical particles and complex experimental reagents have no effective solution thus far. In this experimental context, it is understood that the reaction reagent in aerosol jet printing (AJP) technology uses microsphere droplets as the basic reactor to spray onto the specified substrate, which can greatly improve the sphericity of nanoparticles [6-8]. Customized initial fluorescence patterns can be obtained by controlling the experimental parameters of the AJP technique.

2. Experimental Details

2.1. Preparation of Eu_2O_3 microspheres

The specific process was performed at room temperature. EuCl3·6H2O (99.99% purity, China Aladdin) was added to ultrapure water to prepare a solution of 0.8 mol/L. The equipment includes an Aerosol Jet Printer (HMP, WE Electronics, China), and the schematic is shown in **Figure 1a**. The target pattern can be predrawn using CAD software and entered into the device.

The specific experimental operation steps are as follows. First, an appropriate amount of $EuCl_3$ was

[a*]1574466764@qq.com

placed into a small glass bottle (3 cm in diameter and 10 cm in height), and the bottle was placed into the ultrasonic atomizer (1.7 MHz) to form a uniform aerosol of mist particles. Second, the first pass of N_2 to the glass bottle was intended to drive the aerosol stream. The second pass of N_2 to the terminal of the printing equipment was intended to sheath the aerosol stream so that it was aligned directly with the prefixed glass substrate on the heating table (set at 90°C). The ratio of transport gas and sheath gas was set to 80 sccm:180 sccm in an attempt to prevent the sprayed aerosol gas stream from splashing, reducing the resolution of the plot line, as shown in **Figure 1b**. It is slightly important to note that the substrate chosen for this experiment is a common laboratory glass slide (30 mm*80 mm). The reason is that it has a smaller contact angle and larger surface energy. In this experiment, high-temperature-resistant quartz glass with a similar contact angle and surface energy as ordinary laboratory slides was also chosen as the substrate. Third, the route of aerosol stream injection followed the set pattern and entered the printing device to form the target pattern, as shown in **Figure 1c**. After being printed, the samples were placed into a crucible preheated to 90°C and quickly transferred to a muffle furnace preheated to 90°C. The heating rate was 2°C/min slowly, and then the printed sample was calcined at a constant temperature for 3 hours. Finally, it is vital to naturally cool to room temperature. The calcined sample is shown in **Figure 1c**. **Figure 1d** shows the sample after calcination emitting red light under a UV lamp (λ_{ex}=256 nm). When the sample was printed the sample did not emit any light under the UV lamp (λ_{ex}=256 nm) without calcining.

2.2. Characterization of Eu_2O_3 nanoparticles

The crystal phase composition of the synthesized Eu_2O_3 nanoparticles was determined by a Rigaku SmartLab SE (Japan) X-ray diffractometer using CuKα radiation with a scan velocity of 5°/min. The X-ray diffraction (XRD) data were collected in the range of 10-80°. The whole morphology of Eu_2O_3 nanoparticles was obtained by scanning electron microscopy (SEM, ZEISS Gemini SEM 300) and transmission electron microscopy (TEM, JEOL JEM-F200). The photo of the Eu_2O_3 nanoparticles was recorded with optical microscopy (KEYENCE, VHX-6000, Japan). The photoluminescence spectra and intensity data were measured by a fluorescence spectrometer (F-2700 FL Spectrophotometer, Japan).

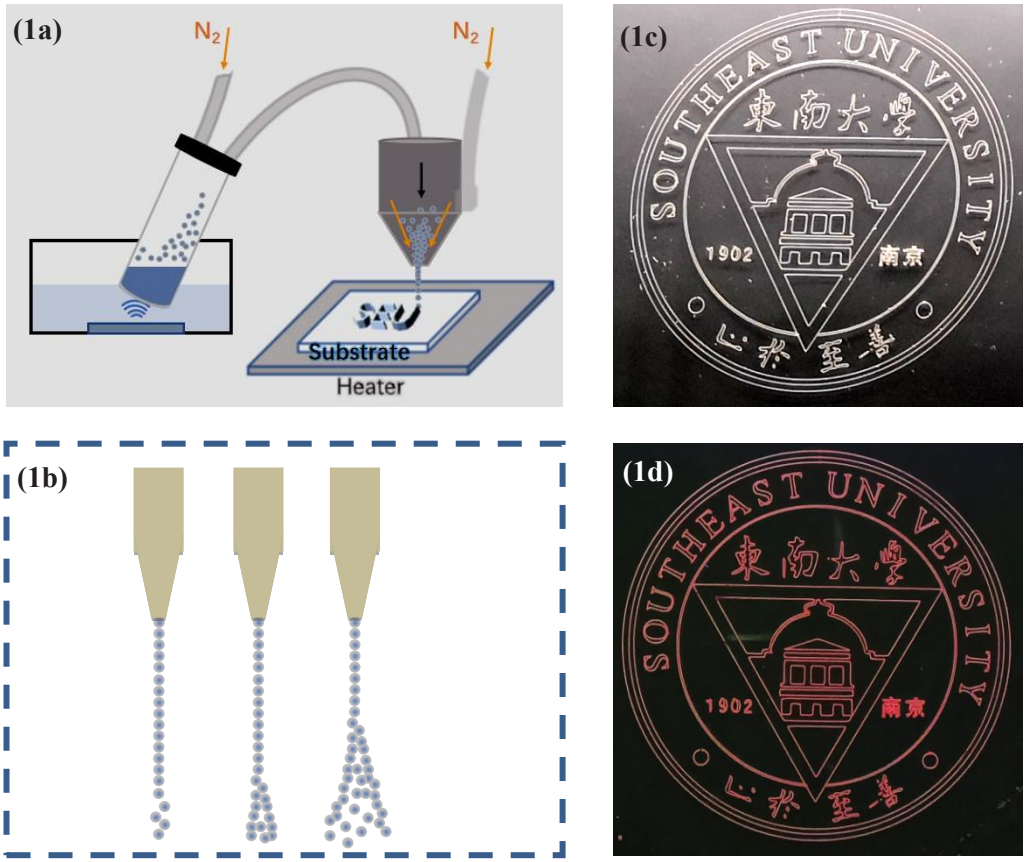

Figure 1. (1a) A schematic of the aerosol jet printer; (1b) A schematic of different focus ratios of the aerosol stream and sheath gas; (1c) Photograph of the printed and calcined sample; (1d) Photograph of the calcined sample under UV light excited at 254 nm.

3. Results and Discussions

3.1 Analysis of XRD

The XRD patterns of Eu_2O_3 at various temperatures are shown in **Figure 2**. All the diffraction peaks of the deposited samples calcined at 1000℃ are in agreement with the Eu_2O_3 C-type phase, which are identical to the standard values of cubic structure Eu_2O_3 (JCPDS No.34-0392) [1]. The XRD patterns of the samples calcined at 400℃~600℃ reveal that a partial phase of the samples is the C-type phase, with the other phases indexed to the B-type phase [8]. From **Figure 2**, the XRD analysis clearly suggests the structural phase transition between C-type and B-type, and thus, it can be concluded that as the calcination temperature increases, the crystallinity becomes better.

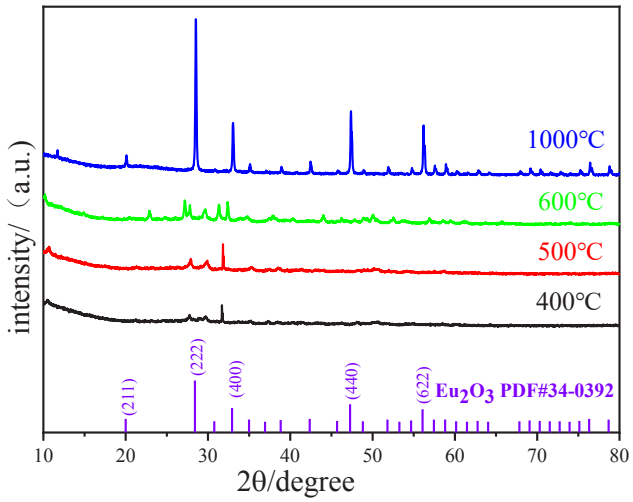

Figure 2. XRD patterns of Eu_2O_3 calcined at 400℃, 500℃, 600℃, and 1000℃.

3.2 Analysis of SEM and TEM

As shown in **Figure 3a**, **3b** and **3c**, the samples calcined at 400℃~600℃ are composed of lamellar-shaped and stick-shaped particles. The shape of these particles gradually becomes spherical when increasing the calcination temperature. **Figure 3d**, **3e** and **3f** correspond to the TEM patterns of the Eu_2O_3 nanoparticles calcined at 400~600℃. The Eu_2O_3 spherical particles calcined at 600℃ are formed by rod-like particles stacked together, accumulating some large pores between particles, which may cause light loss due to light scattering [9-11]. However, the sphericity of Eu_2O_3 nanoparticles calcined at 600℃ is still unsatisfactory, so the author attempted to obtain Eu_2O_3 sphericity samples calcined at 1000℃. **Figure 3g** shows that the SEM results of Eu_2O_3 nanoparticles calcined at 1000℃ are composed of spherical particles. As a corroboration, the TEM results showed that the samples calcined at 1000℃ consist of well-defined microspherical nanostructures with diameters of approximately 100~500 nm, as shown in **Figure 3h**. The lattice fringe is 0.3161 nm, as shown in **Figure 3i**, which is chosen to be the {222} lattice planes of cubic Eu_2O_3 [12, 13]. These results reveal that the pure cubic Eu_2O_3 phase was formed after calcination at 1000℃.

3.3 Analysis of spectra

Figure 4 exhibits the excitation and emission spectra of the Eu_2O_3 nanoparticles at the various calcination temperatures, and there is also a group of fluorescence intensity data of Eu_2O_3 phosphors prepared by the ammonia precipitation method (the calcination temperature is 500℃) as the control group to compare the intensity of luminescence. According to the literature [10-19], the excitation peak wavelength of Eu^{3+} is 393 nm. Therefore, the Eu^{3+} emission spectrum is excited by the wavelength of 393 nm, as shown in **Figure 4a**. The emission peaks of the Eu_2O_3 nanoparticles calcined at 400~600℃ are at 620 nm, 1000℃ and 612 nm, corresponding to the literature, and that obtained by ammonia precipitation is at 628 nm. It is inferred that the shift of the highest emission peak may be related to the phase of Eu_2O_3. The larger the value of the ratio of C-type/(B-type+C-type) in Eu_2O_3 nanoparticles, the closer the wavelength of the peak Eu^{3+} emission spectrum is to 612 nm. In contrast, the wavelength of the peak Eu^{3+} emission spectrum may be extended to 630 nm from 612 nm [15-19].

Figure 4b show that Eu_2O_3 prepared in various environments all have a peak at a wavelength of 393 nm. In the excitation spectrum (**Figure 4b**), in addition to the wavelength of 393 nm, some peaks of Eu_2O_3 prepared under various environments are mainly concentrated at wavelengths of 310 nm and 270 nm. Another peak of Eu_2O_3 calcined at 400℃ or 500℃ is at 310 nm, mainly emitting red light. The minor peak of Eu_2O_3 calcined at 600℃ or 1000℃ or prepared by the ammonia precipitation method is at a wavelength of 270 nm, which is ultraviolet light. It is worth noting that Eu_2O_3 calcined at 600℃ has the highest peak at 270 nm, and the

micropeak is 393 nm. The data of the two peaks are very close, indicating that the electronic transitions are scattered. Therefore, under ultraviolet lamp irradiation (fixed excitation peak of 256 nm), Eu_2O_3 calcined at 600℃ has the weakest luminescence performance, as shown in **Figure 4d**.The emission spectrum of Eu_2O_3 can be obtained, as shown in **Figure 4c**. It can be observed that the peak of Eu_2O_3 calcined at 1000℃ is 612 nm, the peak of Eu_2O_3 calcined at 400~600℃ is 620 nm, and the intensities of peaks distributed to the B-type phase increase with increasing calculation temperature. The peak of Eu_2O_3 obtained by the ammonia precipitation method is 628 nm, consistent with the emission spectrum of Eu^{3+}. The fluorescence of the Eu_2O_3 samples calcined at 1000℃ is much superior to that prepared under other conditions, and the fluorescence performance of Eu_2O_3 prepared by AJP is also much higher than that prepared by ammonia precipitation, as shown in **Figure 4c**, **4d** and **4e**.

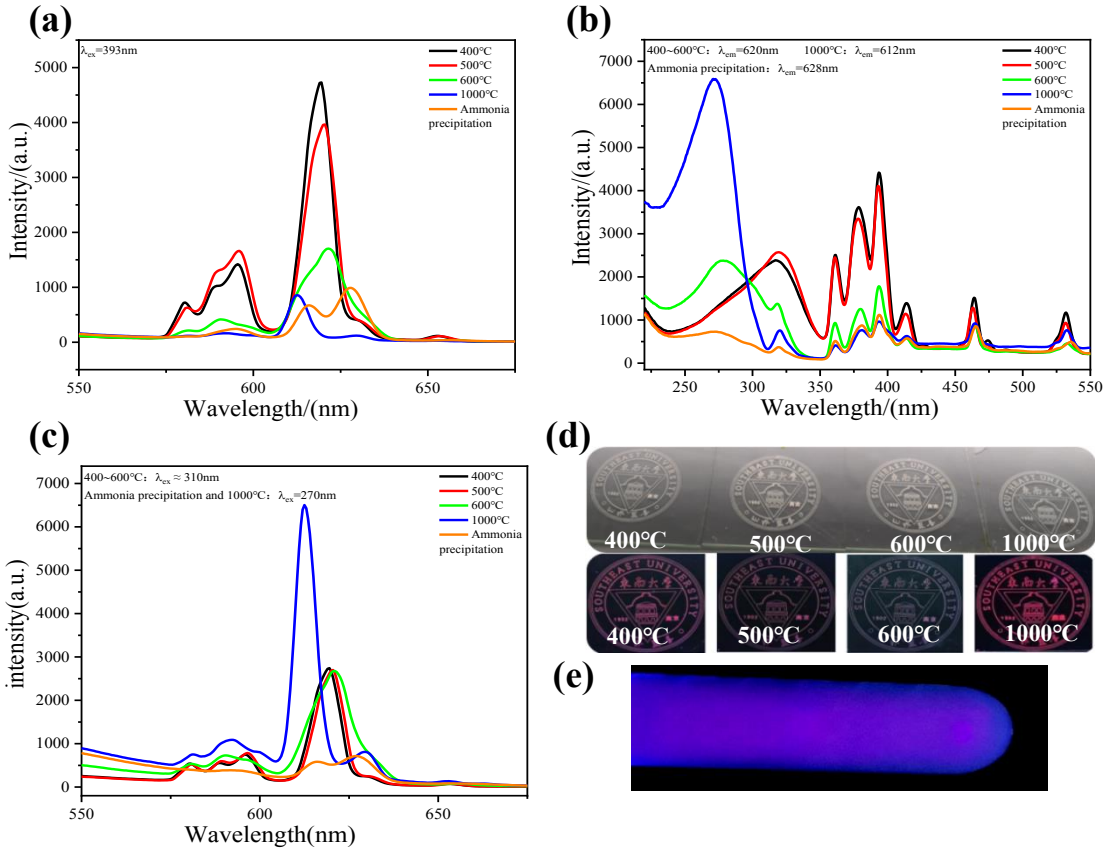

Figure 3. Fluorescence spectra images of Eu_2O_3 calcined at 400℃, 500℃, 600℃, and 1000℃. (a) Emission spectrum, λex=393 nm; (b) excitation spectrum, λem=620 nm, 612 nm or 628 nm; (c) emission spectrum, λex=310 nm or 270 nm; (d) luminescent images of Eu_2O_3 calcined at 400℃, 500℃, 600℃, and 1000℃; (c) luminescent images of Eu_2O_3 prepared by the ammonia precipitation method.

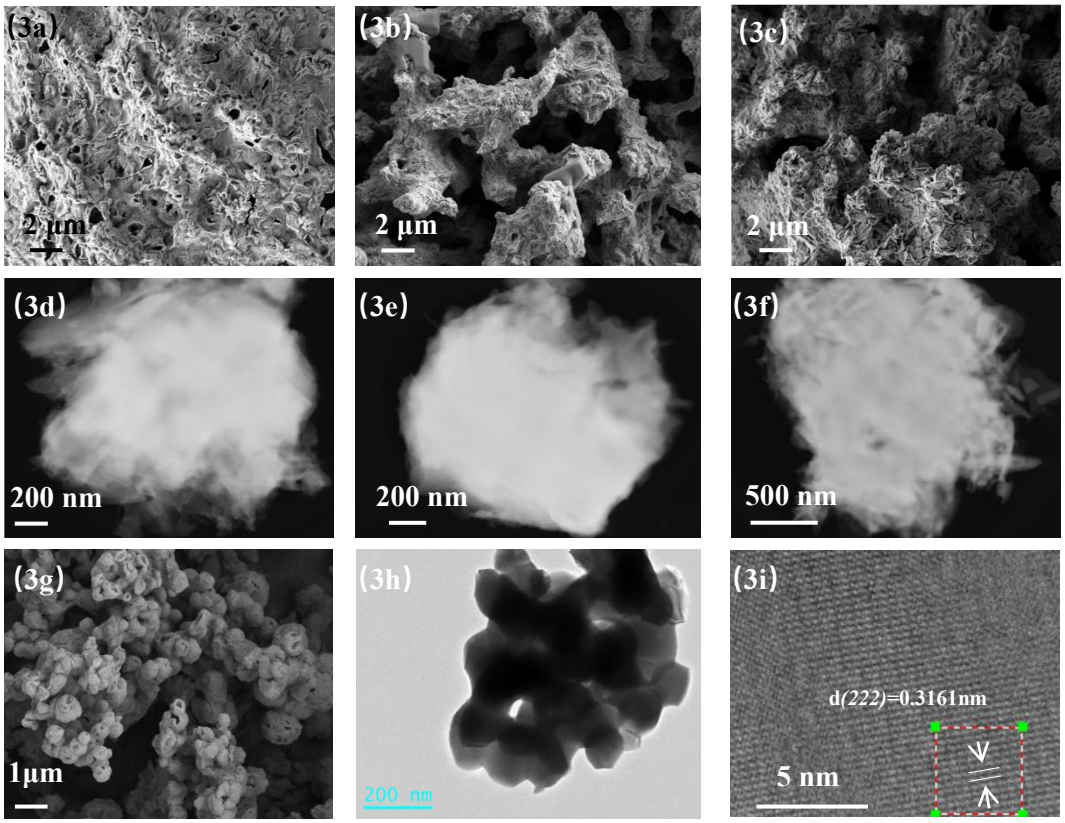

Figure 4. (3a) SEM image of Eu_2O_3 calcined at 400℃; (3b) SEM image of Eu_2O_3 calcined at 500℃; (3c) SEM image of Eu_2O_3 calcined at 600℃; (3d) TEM image of Eu_2O_3 calcined at 400℃; (3e) TEM image of Eu_2O_3 calcined at 500℃; (3f) TEM image of Eu_2O_3 calcined at 600℃; (3 g) SEM image of Eu_2O_3 calcined at 1000℃; (3 h) TEM image of Eu_2O_3 calcined at 1000℃; (3i) Crystal plane of Eu_2O_3 calcined at 1000℃.

4. Conclusion

Eu_2O_3 near-spherical particles are a superior luminescent material with promising prospects for application in opto-electronic fields. The phosphor materials prepared by AJP have excellent morphology and luminescence performance. Their luminescent properties are far higher than those of fluorescent materials prepared by the traditional ammonia precipitation method. The XRD, SEM, TEM and optical drawings demonstrate that C-type Eu_2O_3 near-spherical particles can be synthesized successfully when the calcination temperature is 1000℃. The SEM results showed that the Eu_2O_3 nanoparticles calcined at 1000℃ tended to be spherical. Comparing the fluorescence spectra of Eu_2O_3 prepared by AJP and the ammonia precipitation method, it can be seen that AJP technology has great advantages in the preparation of fluorescent materials with excellent luminescent properties. The microreactor is the microsphere droplet that can improve the sphericity of particles, and the spray route can be customized.

Acknowledgments

This work was financially supported by the Jiangsu Key R&D Plan (6503007555).

References

1. Zhang, L., Luo, J., Wu, M., Jiu, H., & Chen, Q. (2007). Synthesis of Eu2O3 hollow submicrometer spheres through a sol–gel template approach. Materials Letters, 61(23-24), 4452-4455.
2. Golec, P., Żelechowska, K., Karczewska-Golec, J., Karczewski, J., Leśniewski, A., Łoś, M., ... & Kłonkowski, A. M. (2017). Bacteriophages as factories for Eu2O3 nanoparticle synthesis. Bioconjugate Chemistry, 28(7), 1834-1841.
3. Eliseeva, S. V., & Bünzli, J. C. G. (2011). Rare earths: jewels for functional materials of the future. New Journal of Chemistry, 35(6), 1165-1176.
4. Hu, J., Chen, M., Fang, X., & Wu, L. (2011). Fabrication and application of inorganic hollow spheres. Chemical Society Reviews, 40(11), 5472-5491.
5. Lou, X. W., Archer, L. A., & Yang, Z. (2008). Hollow micro-/nanostructures: synthesis and applications. Advanced Materials, 20(21), 3987-4019.
6. Chen, Q. H., Shi, S. Y., & Zhang, W. G. (2009). Study on the structure and luminescent properties of the coordinated Eu2O3 ethanol colloids. Materials Chemistry and Physics, 114(1), 58-62.
7. Liu, J., Wu, C. C., Yang, C. F., & Liou, L. S. (2019). Effect of Eu2O3 Concentration on the Properties of Red-Light-Emitting Sr 1. 5 Ca 0. 5 SiO4

Fluorescent Materials. Nano, 14(09), 1950110.
8. Kishimura, H., Hamada, S., Aruga, A., & Matsumoto, H. (2016). Effect of shock compression on optical and structural properties of Eu2O3 and Y2O3: Eu3+ powders. Journal of Applied Physics, 119(20), 205111.
9. Alfi, N., Rezvani, A. R., Khorasani-Motlagh, M., & Noroozifar, M. (2017). Synthesis of europium oxide-promoted Pd catalyst by an improved impregnation method as a high performance catalyst for the ethanol oxidation reaction. New Journal of Chemistry, 41(19), 10652-10658.
10. Yin, S., Shinozaki, M., & Sato, T. (2007). Synthesis and characterization of wire-like and near-spherical Eu2O3-doped Y2O3 phosphors by solvothermal reaction. Journal of luminescence, 126(2), 427-433.
11. Wakefield, G., Keron, H. A., Dobson, P. J., & Hutchison, J. L. (1999). Synthesis and properties of sub50-nm europium oxide nanoparticles. Journal of colloid and interface science, 215(1), 179-182.
12. Chen, Q. H., Zhang, W. G., & Huang, X. X. (2008). Study on continuous preparation of nano europium oxide ethanol sols decorated in situ by pulsed laser ablation and their luminescence characteristics. Optical Materials, 30(6), 822-826.
13. Wang, S., Gu, F., Li, C., & Lü, M. (2007). Synthesis of mesoporous Eu2O3 microspindles. Crystal Growth and Design, 7(12), 2670-2674.
14. Quesada, A., del Campo, A., & Fernandez, J. F. (2014). Sintering behaviour and translucency of dense Eu2O3 ceramics. Journal of the european ceramic society, 34(7), 1803-1808.
15. Guzman, J. A. L., Alarcón, R. I. S., Alarcón Flores, G., Falcony Guajardo, C., Urby, R. B., Castro, N. C., ... & Carmona Téllez, S. (2018). Microwave-assisted synthesis and characterization of Y 2° 3: Eu (III)-benzoate hybrid nanophosphors. Journal of Nanophotonics, 12(2), 026019-026019.
16. Bosco, G. B., & Tessler, L. R. (2019). Crystal field parameters of the C2 site in Eu2O3. Optical Materials: X, 2, 100028.
17. Wang, T., Wang, S., Wei, Y., Zou, X., Zhang, H., Wang, L., ... & Lv, H. (2020). Preparation and luminescence properties of Eu2O3 doped glass-ceramics containing NaY (MoO4) 2. Journal of the European Ceramic Society, 40(4), 1671-1676.
18. Kaszewski, J., Witkowski, B. S., Wachnicki, Ł., Przybylińska, H., Kozankiewicz, B., Mijowska, E., & Godlewski, M. (2016). Luminescence enhancement in nanocrystalline Eu2O3 nanorods–microwave hydrothermal crystallization and thermal degradation of cubic phase. Optical Materials, 59, 76-82.
19. Chen, W., Joly, A. G., Kowalchuk, C. M., Malm, J. O., Huang, Y., & Bovin, J. O. (2002). Structure, luminescence, and dynamics of Eu2O3 nanoparticles in MCM-41. The journal of physical chemistry B, 106(28), 7034-7041.